Inorganic Chemistry

Article

pubs.acs.org/IC

Exploring the Interaction of N/S Compounds with a Dicopper Center: Tyrosinase Inhibition and Model Studies

Elina Buitrago,[†] Alexandra Vuillamy,[†,▽] Ahcène Boumendjel,[‡] Wei Yi,[‡,∥] Gisèle Gellon,[†] Renaud Hardré,[§] Christian Philouze,[†] Guy Serratrice,[†] Hélène Jamet,[†] Marius Réglier,*[,§] and Catherine Belle*[,†]

[†]Université Grenoble Alpes, DCM, CNRS, F-38000 Grenoble, France

[‡]Université Grenoble Alpes, DPM, CNRS, F-38000 Grenoble, France

[§]Aix Marseille Université, Centrale Marseille, CNRS, ISM2 UMR 7313, Marseille 13397, France

Supporting Information

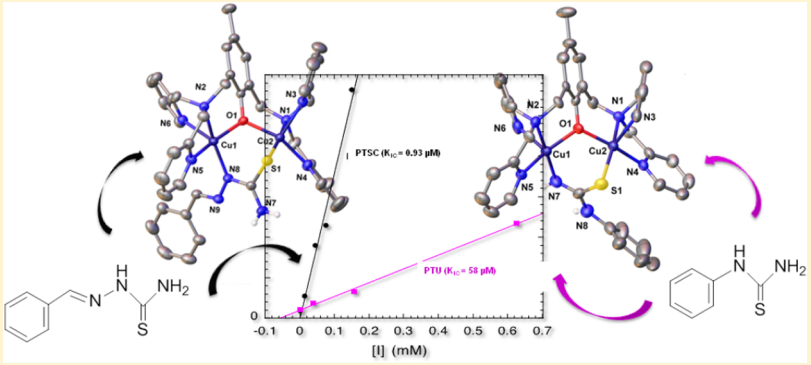

ABSTRACT: Tyrosinase (Ty) is a copper-containing enzyme widely present in plants, bacteria, and humans, where it is involved in biosynthesis of melanin-type pigments. Development of Ty inhibitors is an important approach to control the production and the accumulation of pigments in living systems. In this paper, we focused our interest in phenylthiourea (PTU) and phenylmethylene thiosemicarbazone (PTSC) recognized as inhibitors of tyrosinase by combining enzymatic studies and coordination chemistry methods. Both are efficient inhibitors of mushroom tyrosinase and they can be considered mainly as competitive inhibitors. Computational studies verify that PTSC and PTU inhibitors interact with the metal center of the active site. The K_{IC} value of 0.93 μM confirms that PTSC is a much more efficient inhibitor than PTU, for which a K_{IC} value of 58 μM was determined. The estimation of the binding free energies inhibitors/Ty confirms the high inhibitor efficiency of PTSC. Binding studies of PTSC along with PTU to a dinuclear copper(II) complex ($[Cu_2(\mu\text{-BPMP})(\mu\text{-OH})](ClO_4)_2$ (**1**); H-BPMP = 2,6-bis-[bis(2-pyridylmethyl)aminomethyl]-4-methylphenol) known to be a structural and functional model for the tyrosinase catecholase activity, have been performed. Interactions of the compounds with the dicopper model complex **1** were followed by spectrophotometry and electrospray ionization (ESI). The molecular structure of **1**-PTSC and **1**-PTU adducts were determined by single-crystal X-ray diffraction analysis showing for both an unusual bridging binding mode on the dicopper center. These results reflect their adaptable binding mode in relation to the geometry and chelate size of the dicopper center.

INTRODUCTION

Tyrosinase (Ty, EC 1.14.18.1) belongs to the type-3 family of the copper-containing enzymes, along with catechol oxidase (CO, EC 1.10.3.1).[1] Ty is widely distributed throughout plants, fungi, bacteria, and mammals, while CO is mainly found in plants. The common feature of these enzymes is the presence of an active site composed by two close Cu atoms each coordinated by three histidine residues. Comparison of crystallographic structures from different forms of Ty and CO shows that the catalytic active sites are highly conserved while the analysis of the second coordination sphere point out important differences explaining thus the different reactivity.[2] While Ty catalyzes the hydroxylation of phenolic compounds to *o*-diphenols (phenolase activity) and the subsequent oxidation into quinones (catecholase activity), CO only catalyzes the *o*-diphenols oxidation (see Figure 1a).

The X-ray structures of tyrosinases have been reported from fungal,[2a,3] plant and bacteria[2f,4] sources. Different states, which could be referred as different stages of the catalytic cycle, have been evidenced: a *met* state (Cu^{II}–Cu^{II}), a reduced *deoxy* state (Cu^{I}–Cu^{I}), and an *oxy* state with a dioxygen bound to the dicopper center (Cu^{II}–O_2^{2-}–Cu^{II}). In the *met* state, the two cupric ions (Figure 1b) are bridged by hydroxido (aqua) ligands, providing an antiferromagnetic coupling between the Cu^{II} ions that is characteristic for type-3 copper enzymes. For

Received: July 28, 2014
Published: November 21, 2014

   dx.doi.org/10.1021/ic501829s | *Inorg. Chem.* 2014, 53, 12848−12858

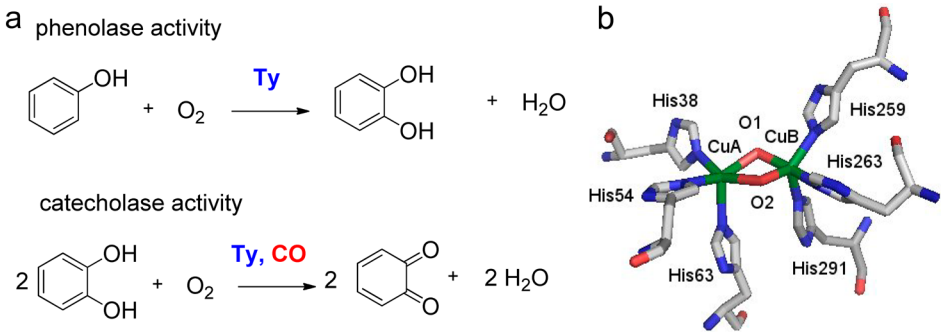

Figure 1. (a) Ty and CO-catalyzed oxidations and (b) the active site of *Streptomyces castaneoglobisporus* bacterial tyrosinase (*met* form II, PDB code: 2AHK).

Chart 1. Isolated and X-ray Characterized Adducts of 2-Hydroxypyridine-*N*-oxide (HOPNO)[17] and Kojic Acid (KA)[18] with Model Complex 1, and Chemical Structures of Phenylthiourea (PTU) and Phenylmethylene Thiosemicarbazone (PTSC) Used in This Work

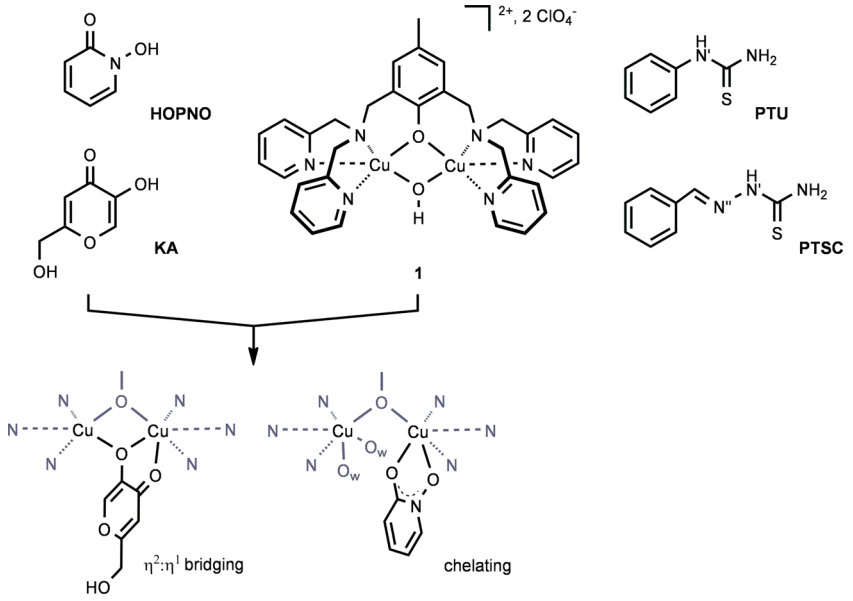

catechol oxidases isolated from plant[5] and fungus,[2b] analogous states have also been characterized by X-ray crystallography.

In all organisms, Ty and CO are involved in the biosynthesis of pigments, which results in the autopolymerization of quinones formed by the Ty/CO oxidation of phenol and catechol precursors. In mammals, Ty is involved in the two-step oxidation of L-tyrosine into L-DOPA (L-3,4-dihydroxyphenylalanine) and dopaquinone, the key products for melanin pigment biosynthesis.[6]

Development of Ty inhibitors is an important approach not only to decipher the catalytic mechanism of Ty but also to control the production and the accumulation of phenolic pigments in living systems. Inhibitors of Ty find applications in food industry (antibrowning),[7] cosmetics (skin-lightening),[8] and therapeutics.[9] Phenylthiourea (PTU, Chart 1) has been shown to inhibit tyrosinase[10] and catechol oxidase.[11] Furthermore, the crystal structure of catechol oxidase from sweet potatoes (*Ib*CO), reported in the *met* form with bound phenylthiourea,[5a] has unambiguously evidenced that PTU binds the dicopper center in the active site (see Figure 4a, presented later in this work) as a bridging ligand with the S atom of the PTU replacing the bridging hydroxido. Exploring different copper-binding groups appears to be an attractive strategy to develop new scaffolds, which better target the Ty metal-active site for more selective and potent inhibitors. In previous reports, thiosemicarbazones (TSCs) have shown significant potential as tyrosinase inhibitors.[12] Furthermore, these molecules are often excellent chelators of transition metals, because of their N−N−S tridentate coordination scaffold. Because their metal complexes often possess potent medicinal properties, a very rich literature exists exploring the chemistry and biology of metal-bound thiosemicarbazones, particularly mononuclear Cu^{II}-TSC.[13] Taking advantage of above information, we focused our studies on the parent compounds—phenylmethylene thiosemicarbazone (PTSC)[12j,14] and PTU,[10,12a,14b] recognized as mushroom tyrosinase and/or melanogenesis inhibitors. The complexation can be diverse as TSCs can act as a anionic or neutral, monodentate, chelating, or bridging ligands.

To gain more insight into the interaction mode of these compounds with the enzyme and to determine the inhibition features, we have determined the inhibition constants of PTSC and PTU on enzymatic oxidation of L-DOPA by mushroom tyrosinase. Furthermore, metalloenzyme model complexes are recognized as an effective preliminary approach[15] to provide fundamental chemical insights into competitive inhibitor

dx.doi.org/10.1021/ic501829s | *Inorg. Chem.* 2014, 53, 12848−12858

Table 1. Crystallographic Data for 1-PTSC·$2C_3H_6O$, 1-ClO_4·C_4H_8O·H_2O, and 1-PTU·C_4H_8O

compound	1-PTSC·$2C_3H_6O$	1-ClO_4·C_4H_8O·H_2O	1-PTU·C_4H_8O
formula	$[Cu_2(C_{41}H_{41}ON_9S)](ClO_4)_2\cdot(C_3H_6O)_2$	$[Cu_2(C_{33}H_{33}ClO_5N_6)](ClO_4)\cdot C_4H_8O\cdot H_2O$	$[Cu_2(C_{40}H_{40}ON_8S)](ClO_4)_2\cdot C_4H_8O$
F_w	1150.02	945.75	1078.94
morphology	brown	green	brown-red
crystal size	0.56 mm × 0.51 mm × 0.24 mm	0.38 mm × 0.26 mm × 0.06 mm	0.30 mm × 0.25 mm × 0.16 mm
crystal system	triclinic	triclinic	triclinic
space group	$P\bar{1}$	$P\bar{1}$	$P\bar{1}$
a	11.368(2) Å	10.409(5) Å	9.976(2) Å
b	12.587(3) Å	14.377(5) Å	10.682(2) Å
c	18.617(4) Å	15.537(5) Å	22.847(5) Å
α	87.41(3)°	98.744(5)°	97.76(3)°
β	75.25(3)°	107.054(5)°	102.21(3)°
γ	85.64(3)°	108.745(5)°	103.23(3)°
unit-cell volume	2567.6(9) $Å^3$	2025.6(14) $Å^3$	2293.2(8) $Å^3$
density, D_x	1.487 g cm^{-3}	1.551 g cm^{-3}	1.563 g cm^{-3}
temperature, T	200 K	200 K	200 K
Z	2	2	2
μ	1.040 mm^{-1}	1.248 mm^{-1}	1.157 mm^{-1}
total reflections	57958	25222	40933
unique reflections	14901	7039	10084
observed reflections	10940 ($F > 2\sigma$)	5018 ($F > 2\sigma$)	7898 ($F > 2\sigma$)
R_{int}	0.0319	0.0624	0.0791
R^a	0.0422	0.0928	0.0947
$R(w)^a$	0.0956	0.2573	0.2216
goodness of fit, S	1.108	1.139	1.205
$\Delta\rho_{min}/\Delta\rho_{max}$	−0.756/0.638 e $Å^{-3}$	−0.885/1.524 e $Å^{-3}$	−0.783/0.806 e $Å^{-3}$

[a]Refinement based on F, where $w = 1/[\sigma^2(F_o)^2 + (0.0435p)^2 + 2.3172p]$, with $p = (F_o^2 + 2F_o^2)/3$ for 1-PTSC·$2C_3H_6O$; $w = 1/[\sigma^2(F_o)^2 + (0.0838p)^2 + 34.5554p]$ with $p = (F_o^2 + 2F_o^2)/3$ for 1-ClO_4·C_4H_8O·H_2O and $w = 1/[\sigma^2(F_o)^2 + (0.0000p)^2 + 27.3494p]$, with $p = (F_o^2 + 2F_o^2)/3$ for 1-PTU·C_4H_8O.

binding features. Many Cu_2-based models with catecholase activity have been reported,[1e,16] but only few relevant experimental structures with coordinated inhibitor have been reported. Interestingly, adducts between complex **1** and inhibitors such as kojic acid (KA) or 2-hydroxypyridine (HOPNO) have been reported (Chart 1). Both inhibitors exhibit different binding modes. Deprotonated OPNO chelates only one Cu atom of **1** in a bidentate mode,[17] while deprotonated KA displays a bidentate and bridging η^2:η^1 coordination[18] on the dicopper center.

However, there is no example where the various possible coordination modes of N/S compounds including PTU and TSCs have been analyzed and structurally characterized. In this way, using the binuclear copper(II) complex $[Cu_2(\mu\text{-BPMP})(\mu\text{-OH})](ClO_4)_2$ (**1**; H-BPMP = 2,6-bis-[bis(2-pyridylmethyl)-aminomethyl]-4-methylphenol, Chart 1) known as a structural and functional model of the catecholase activity of Ty and CO,[19] we have explored the binding mode of PTU and PTSC. This information and the related properties will contribute to a better understanding of the inhibition mechanisms.

EXPERIMENTAL SECTION

General. All reagents were purchased from commercial sources and used as received. Solvents were distilled by standard methods before use.

[Caution: Although no problems were encountered, suitable care and precautions should be taken when handling the perchlorate salts.]

The thiosemicarbazones (TSCs) were synthesized according to literature procedures.[12j,20] ESI mass spectra were recorded on an Esquire 300 Plus Bruker Daltonis system or a ZQ 2000, MK II Z-spray from Waters fitted with a syringe pump. HR-MS were recorded on a FT-ICR mass spectrometer 7T hybrid FTICR Apex-Q spectrometer (Bruker Daltonis). Ultraviolet−visible light (UV-vis) analysis were obtained using a Cary 50 spectrophotometer operating in the 200−1000 nm range with quartz cells. The temperature was maintained at 25 °C with a temperature control unit. The spectral parameters for **1**-PTSC and **1**-PTU were determined from the electronic spectra calculated from the refinement of absorbance data by the Specfit program.[21] ^1H NMR spectra were recorded on a Bruker Model Avance 400 spectrometer at 323 K with the deuterated solvent as a lock. X-band EPR spectra were recorded at 100 K with a Bruker ESP EMX Plus spectrometer equipped with a nitrogen-flow cryostat and operating at 9.3 GHz (X-band).

Synthesis. *Synthesis of $[Cu_2(\mu\text{-BPMP})(\mu\text{-PTSC-}\kappa N'\text{:}\kappa S)](ClO_4)_2$ (**1**-PTSC).* To a solution of complex **1**[19] (4.5 mg, 5.2 μmol, 1 equiv) in acetone (1 mL) and acetonitrile (10 drops) was added a solution of phenylmethylene thiosemicarbazone (3.9 mg, 21.8 μmol, 4 equiv) in acetone (0.2 mL). A slow diethyl ether/THF diffusion of the solution leads to crystallization after 1 week. Brown crystals of **1**-PTSC·$2C_3H_6O$ suitable for X-ray diffraction analysis were obtained together with others crystals. (See Figure S1 in the Supporting Information (ESI).) The brown crystals were collected one by one from the batch. Electrospray ionization−mass spectroscopy (ESI-MS) (CH_3CN), m/z: $z = 1$, 934 = $(M - ClO_4)^+$, $z = 2$, 417 = $(M - 2ClO_4^-)^{2+}$. UV-vis (H_2O/DMSO 70/30), λ_{max}, nm (ε, M^{-1} cm^{-1}): 432 (∼410), 698 (∼289). HR-MS (ESI) Calcd. (m/z: $z = 1$) for $[C_{41}H_{41}N_9O_5SClCu_2]^+$: 932.12264. Found: 932.12579 (spectrum shown in the ESI (Figure S2)), Calcd (m/z: $z = 2$) for $[C_{41}H_{41}N_9OSCu_2]^{2+}$: 416.58679. Found:

dx.doi.org/10.1021/ic501829s | Inorg. Chem. 2014, 53, 12848−12858

416.58659. The green platelet crystals of $[Cu_2(\mu\text{-BPMP})(\mu\text{-}ClO_4\text{-}\kappa O{:}\kappa O')](ClO_4)$ were collected one by one from the batch. Anal. Calcd for $C_{33}H_{33}Cl_2Cu_2N_6O_9{\cdot}0.5C_3H_6O$: C, 46.84; H, 4.10; N, 9.50. Found C, 46.50; H, 4.22; N, 9.14.

Synthesis of $[Cu_2(\mu\text{-BPMP})(\mu\text{-PTU-}\kappa N{:}\kappa S)](ClO_4)_2$ (1-PTU). To a solution of complex **1**[19] (2 mg, 2.3 μmol, 1 equiv) in acetonitrile (1 mL) was added a solution of phenylthiourea (3.5 mg, 23 μmol, 10 equiv) in ethanol (2 mL). The solution was stirred for 30 min. A slow THF diffusion of the solution leads to crystallization after 3 weeks. Brown-red crystals of **1**-PTU·THF suitable for XRD analysis were obtained, together with dark green crystals of complex **1**. The brown-red crystals were collected one by one from the batch. Anal. Calcd for $C_{40}H_{40}Cl_2Cu_2N_8O_9S$: C, 47.72; H, 4.00; N, 11.13. Found C, 47.54; H, 4.13; N, 10.97. ESI-MS (CH_3CN), m/z: z = 1, 905 = (M - ClO_4^-). UV-vis (H_2O/DMSO 70/30)), λ_{max}, nm (ε, M^{-1} cm^{-1}): 440 (∼240), 720 (∼120).

Crystal Structure Determinations and Refinements. Measurements were made on a Bruker−Nonius Kappa CCD diffractometer with graphite monochromatized Mo(Kα) radiation (λ = 0.71073 Å). The crystal data and details of the data collections are given in Table 1. Crystallographic structures were solved using direct methods implemented by ShelxS-97.[22] Refinement was performed using ShelxL-97[22] run under Olex2.[23] C, N, O, S, Cl, and Cu atoms were refined anisotropically by the full matrix least-squares method. H atoms were calculated on idealized positions and constrained on their bearing atoms. For **1**-PTU·C_4H_8O, the obtained model did not refine well, because of twinning. The selected crystal revealed the following twin law:

$$\begin{pmatrix} -0.999 & -0.002 & 0.004 \\ 0.001 & -1.000 & -0.002 \\ 1.005 & 0.796 & 0.995 \end{pmatrix}$$

with a ratio of 29.37% vs 70.6% corresponding to two different lattices rotated by 179.87°. For each, the data were integrated separately, corrected for absorption and finally merged into an entire hklf5 file format using TWINABS.[24]

Determination of Stability Constants. The binding constants of the inhibitor to the dinuclear Cu(II) complex were determined by spectrophotometric titration in water/DMSO 70/30 (v/v) solutions buffered at pH 7.0 with 100 mM HEPES. The titrations were carried out by adding small aliquots of a concentrated solution of the inhibitor to solution of complex **1**. The spectral data were processed with the SPECFIT/32 Global Analysis System (Spectrum Software Associates),[21] adjusting the equilibrium constants and the corresponding molar extinction coefficient of the species at equilibrium. Details and titration curves of complex **1** by PTU and PTSC are given in the Supporting Information (Figure S3).

Biological Evaluation. PTU and PTSC were assayed as inhibitors of tyrosinase purified from the *Agaricus bisporus* mushroom. Crude extract of the mushroom tyrosinase (6.4 mg), purchased from Sigma (St. Louis, MO, USA), was dissolved in 50 mM phosphate buffer (5 mL, pH 7.0) and purified on Q-sepharose FF chromatography by a gradient of NaCl from 0 to 1.0 M.[25] Purity of tyrosinase was checked with SDS-PAGE; the purified tyrosinase exhibits only two bands at molecular weights of MW = ca. 14 kDa and 45 kDa. The Ty activity was checked with spectroscopic method using L-DOPA as substrate *Agaricus bisporus* mushroom tyrosinase exhibited a K_M value of 0.302 ± 0.033 mM and a V_{max} value of 14.0 ± 0.3 μM min^{-1}.

All compounds were dissolved in DMSO stock solution 10%. Phosphate buffer pH 7.0 was used to dilute the DMSO stock solution of the compounds. Six units of mushroom tyrosinase (6.4 μg/mL) were first preincubated with PTU and PTSC, in 50 mM phosphate buffer (pH 7.0), for 5 min at 25 °C. Then, the L-DOPA (0.1−5 mM) was added to the reaction mixture and the enzyme reaction was monitored by measuring the change in absorbance at 475 nm of the DOPAchrome for 3 min.

Theoretical Calculations. *QM Calculations.* QM calculations were based on DFT and have been performed with the Gaussian09 package.[26] To estimate the exchange coupling constants, single-point energy calculations on crystal structures of complexes **1**-PTU and **1**-PTSC were performed using the B3LYP functional and the 6-311G* basis set on all atoms. High-spin and broken-symmetry calculations were done, and the Yamagachi formula[27] was used.

Docking Protocol. The calculations were made using the recently resolved *Agaricus bisporus* mushroom tyrosinase (PDB code: 2Y9X).[2a] The addition of H atoms leads to the protonation of all histidines on the δ nitrogen atom, whereas the aspartate and glutamate residues remain deprotonated and the arginine and lysine residues are positively charged. Then, the crystal structures of **1**-PTSC, **1**-PTU were aligned with the active site of the enzyme with the fit atom tool of Sybyl version 8.0.[28] Alignment was done between the nitrogen Nε of histidine and Cu atoms from the enzyme and the pyridine nitrogen and Cu atoms of the complexes.

The system was solvated with a truncated octahedral box of TIP3PBOX water molecules (10 Å radius) and neutralized with Na^+ ions. For the MM simulations, the Amber99SB force field was used in conjunction with specific parameters developed for Cu ions, histidine residues, and the hydroxy group linked to the Cu atoms in the active site.[29] For PTSC and PTU, parameters were constructed with the module Antechamber of Amber12 with the GAFF force field. During the simulations, constraints were applied to freeze the positions of these atoms (the Cu ions, the histidine residues, and the hydroxy group). For each complex, MM simulations of 2 ns were performed. After 0.5 ns of equilibration, 50 snapshots were selected to calculate the relative binding affinities for the two inhibitors using the MM-PBSA method in Amber12.[29]

$$\Delta G = G_{complex} - G_{protein} - G_{ligand} \quad (1)$$

$$G(X) = E_{MM}(X) + G_{PB}(X) + G_{SA}(X) \quad (2)$$

where E_{MM} is the molecular mechanical gas-phase energy, G_{PB} the electrostatic solvatation energy calculated in solving the Poisson−Boltzmann equation, and G_{SA} a nonpolar solvation energy proportional to the solvent-accessible surface area. Having compared two structurally close ligands binding the same protein, changes in solute entropy were not included in the calculations.

RESULTS AND DISCUSSION

Effect of Inhibitors on Mushroom Ty-Catalyzed L-DOPA Oxidation. The effect of PTSC and PTU compounds on the oxidation of L-DOPA by mushroom Ty was studied. We first determined that the Ty inhibition was concentration-dependent (see Figure 2 and Table 2). For these determinations, we used L-DOPA concentrations 30−20 times lower than the K_M value ([L-DOPA] = 0.1−0.15 mM vs K_M = 0.300−0.247 mM) giving an approximation of the inhibition constant

Table 2. *Agaricus bisporus* Mushroom Tyrosinase Inhibition Constants Values with Standard Deviations Determined for Compounds PTSC and PTU[a]

compound	K_{IC} (μM)[b]	K_{IU}(μM)[b]
PTU	58 ± 12	450 ± 100
HOPNO	1.8[c]	
PTSC	0.93 ± 0.10	93 ± 3

[a]Conditions: 50 mM phosphate buffer (pH 7.0 at 25°C), L-DOPA (0.1−5 mM) oxidation monitored in the presence of PTSC and PTU by measuring the change in absorbance at 475 nm for 3 min. [b]For comparison, kojic acid is reported in the literature as a mixed inhibitor with K_I in the range of 20 μM.[32] [c]Data taken from ref 17.

K_I, which allowed comparison of the efficiency of the inhibitors. With an IC_{50} value of 7.5 μM, PTSC appears to be a much more potent inhibitor than PTU, which under the same conditions exhibits an IC_{50} value of 97 μM. The kinetic behavior of the PTSC and PTU compounds was then studied on mushroom Ty-catalyzed oxidation of L-DOPA. For both compounds, the initial rate constant was determined at various L-DOPA concentrations and for various concentrations of inhibitors (see Figures S4a and S6a in the ESI).

A Michaelis−Menten treatment of the collected data leads to a set of V_{max}^{app} and K_M^{app} (see Figures S4b and S6b in the ESI) that was used for the determination of the inhibition constants.[30] In the first approximation, we considered PTSC and PTU as mixed inhibitors. For mixed inhibitors, the V_{max}^{app} and K_M^{app} constants are expressed as a function of inhibitor concentration:

$$V_{max}^{app} = \frac{V_{max}}{1 + \frac{[I]}{K_{IU}}} \quad (3)$$

$$\frac{1}{V_{max}^{app}} = \frac{1}{V_{max}} + \frac{[I]}{V_{max}K_{IU}} \quad (4)$$

$$K_M^{app} = \frac{K_M\left(1 + \frac{[I]}{K_{IC}}\right)}{1 + \frac{[I]}{K_{IU}}} \quad (5)$$

$$\frac{K_M^{app}}{V_{max}^{M}} = \frac{K_M}{V_{max}} + \frac{K_M[I]}{V_{max}K_{IC}} \quad (6)$$

where K_{IC} is the competitive component of the inhibition and K_{IU} the uncompetitive component.

The macroscopic kinetic features for the competitive inhibition (K_{IC}) and the uncompetitive inhibition (K_{IU}) were determined from the set of V_{max}^{app} and K_M^{app} values. According to eq 6, the linear regression of the $1/V_{max}^{app}$ vs $[I]$ plot leads to the K_{IU} component of the inhibition (see Figures S5a and S7a in the ESI). The same treatment according to eq 6, the K_M^{app}/V_{max}^{app} vs $[I]$ plot leads to the K_{IC} component of the inhibition (see Figure 2b, as well as Figures S5b and S7b in the ESI).

PTSC and PTU both exhibit mixed inhibition features (see Table 2) with the competitive contribution significantly higher, compared to the uncompetitive one, showing that they can be considered mainly as competitive inhibitors. The mixed-type inhibition was already observed with mushroom Ty and aurones compounds in a previous report.[31] Because of the heterotetrameric structure of the mushroom Ty, this behavior suggests a multiple binding site for inhibitors. The K_{IC} value of 0.93 μM confirms that PTSC is a much better inhibitor than PTU, for which a K_{IC} value of 58 μM was determined (Figure 2b). Compared to HOPNO and KA (Table 2), PTSC is an efficient inhibitor for mushroom Ty with one of the best features reported in the literature.

Binding Studies. The evaluation of the inhibition properties of PTU and PTSC evidence that these compounds interact with the Cu ions in the binuclear active site of the enzyme. To complete the present work, we investigated the molecular interactions of model complex **1** and the mentioned inhibitors.

Binding Constant Determinations. The UV-vis spectrum of complex **1** in H_2O/DMSO (70/30, v/v, buffered at pH 7 (HEPES 100 mM)) is characterized by a ligand-to-metal charge transfer (LMCT) transition between the bridging phenoxo and Cu ions at 410 nm (ε = 295 M^{-1} cm^{-1}) and a d-d transition at 730 nm (ε = 230 M^{-1} cm^{-1}). Addition of inhibitors (PTSC and PTU) to a solution of dicopper complex **1** results with a smaller decrease of the d-d bands absorption in the 700 nm region along in the growth of a shoulder to the phenoxo-CT to copper band (~440 nm region) (Figure S3 in the ESI). The former is assigned to a S → Cu^{II} LMCT, since similar LMCT bands have

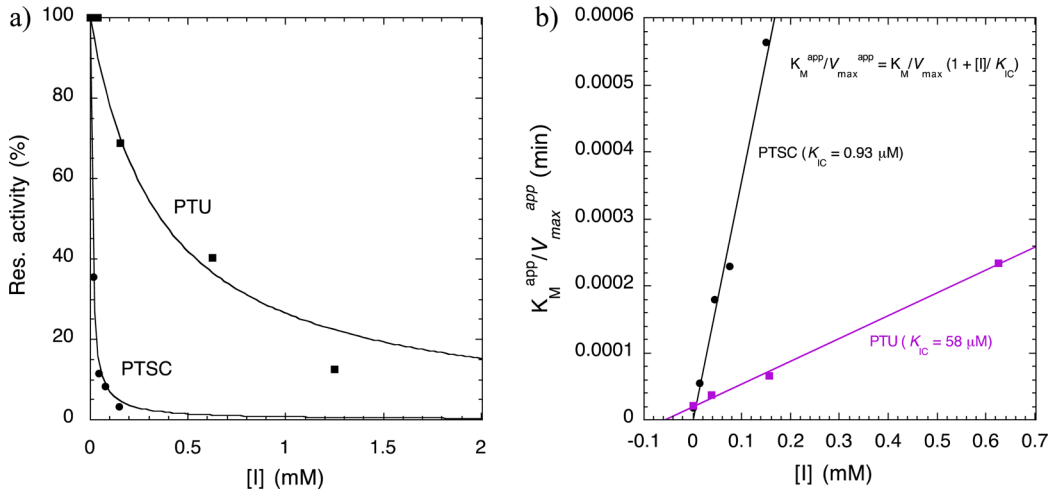

Figure 2. Inhibition of mushroom Ty-catalyzed oxidation of L-DOPA by PTSC and PTU: (a) concentration-dependent inhibition for PTU at [L-DOPA] = 0.1 mM and for PTSC at [L-DOPA] = 0.15 mM; (b) K_M^{app}/V_{max}^{app} vs $[I]$ plots used for the determination of K_{IC}.

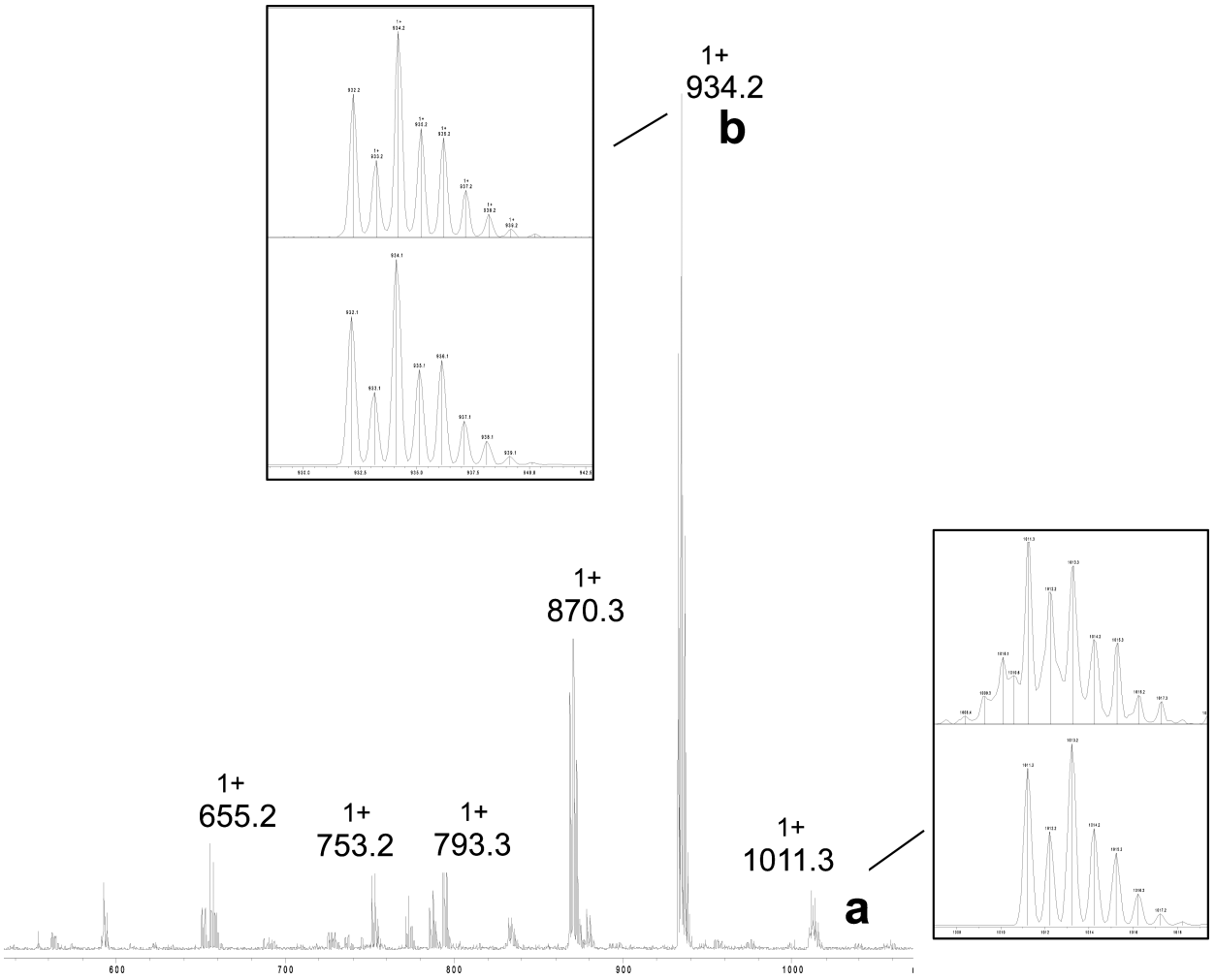

Figure 3. ESI-MS spectrum of solution of **1** and PTSC (ratio 1:7) in acetonitrile; $[Cu_2(BPMP)(PTSC)_2]^+$ (a) and $[Cu_2(BPMP)(PTSC)](ClO_4)^+$ (b); with the experimental (top) and calculated (down) isotopic distribution for fragments **a** and **b**.

also been observed in most copper complexes derived from sulfur-donor ligands such as TSCs.[13a] The refinement of the absorbance data versus inhibitor concentration was performed by the Specfit program.[21] The two models of 1:1 and 1:2 stoichiometry for the adduct complex **1**-inhibitor were tried separately, as well as a mixture of both. The best refinement was obtained by considering only the 1:2 adduct ($\Sigma(A_{exp} - A_{calc})^2$ of the fits was 10^{-2}–10^{-3}, whereas it was 10^{-1}–10^{-2} for the 1:1 stoichiometry or presence of both 1:1 and 1:2). The determined binding constants (K_b [M^{-1}]) indicate weak interactions with the dicopper center (log K_b = 5.49 ± 0.05 and 6.5 ± 0.03, respectively, for PTU and PTSC). Besides, PTU and PTSC display a high affinity for mushroom Ty (see above) suggesting important second-sphere interactions of PTU and PTSC with amino-acid residues in the enzyme. This is supported by X-ray structure of *Ib*CO-PTU, which points out some important interactions of PTU with CO amino acid residues (i.e., van der Waals interactions between the Phe261, Ile241, His244 lining the hydrophobic cavity) and reveals that important second-sphere interactions with amino acid residues contribute to the stabilization of PTU in the binding pocket.[5a]

ESI-MS. ESI-MS analysis of the binuclear copper(II) complex $[Cu_2(\mu\text{-BPMP})(\mu\text{-OH})](ClO_4)_2$ (**1**) in solution treated with PTSC suggests the presence of two possible adducts. Figure 3 displays two featured signals for a mixture of **1** and PTSC (1:7 ratio) in acetonitrile. We observed the fragment centered at m/z = 1013 (z = 1, $[Cu_2(BPMP)(PTSC)_2]^+$, **a**) corresponding to the adduct with two deprotonated PTSC bound on **1** and the fragment corresponding to the 1:1 adduct (m/z = 934 (z = 1, $[Cu_2(BPMP)(PTSC)](ClO_4)^+$, **b**). The corresponding characteristic isotopic distribution patterns are shown in Figure 3.

ESI-MS analysis from a solution of **1** and PTU (1:10 ratio) in CH_3CN displays a fragment at m/z = 905 (z = 1, $[Cu_2(BPMP)(PTU)](ClO_4)^+$, corresponding to the adduct with one deprotonated PTU bound on **1** (spectrum with the observed/theoretical isotopic patterns distribution for the fragment at m/z = 905 is shown in the ESI (Figure S9)). Fragments corresponding to the 1:2 adduct were not observed under these conditions.

Isolated Adducts. Reaction of **1** with PTSC (1:4 ratio) in acetone/acetonitrile and slow vapor diffusion of ether affords a crystalline material after 1 week where brown-red crystals in form of prism are found, together with green crystals (see Figure S1 in the ESI). Crystallographic analysis confirms that the brown crystals are adduct **1**-PTSC (Figure 4b) and the green ones are complex **1**, where the bridging OH has been replaced by a bridging perchlorate (Figure 4a).

The reaction of complex **1** in acetonitrile with PTU (1:10 ratio) in ethanol and slow vapor diffusion of THF afford a crystalline material after three weeks. Brown crystals of **1**-PTU

dx.doi.org/10.1021/ic501829s | *Inorg. Chem.* 2014, 53, 12848–12858

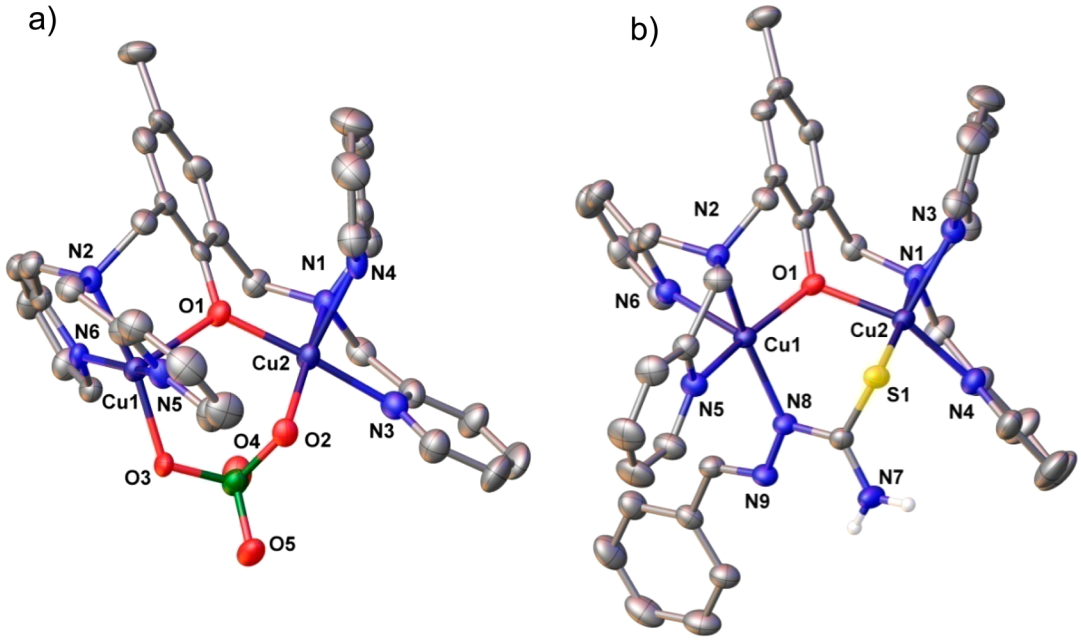

Figure 4. (a) Molecular structure of the cation $[Cu_2(\mu\text{-BPMP})(\mu\text{-}ClO_4\text{-}\kappa O{:}\kappa O')]+$ (description and selected bond lengths and angles are given in the ESI), and (b) molecular structure of the cation of **1**-PTSC. Hydrogen atoms (except on the nitrogen in PTSC), counterions and solvent molecules have been omitted for clarity. Selected bond lengths: Cu1···Cu2, 3.378 Å; Cu1−O1, 1.9850(16) Å; Cu1−N8, 2.0292(19) Å; Cu1−N6, 2.260(2) Å; Cu1−N2, 2.0709(19) Å; Cu1−N5, 2.039(2) Å; Cu2−S1, 2.3700(11) Å; Cu2−O1, 1.9521(16) Å; Cu2−N1, 2.081(2) Å; Cu2−N3, 2.153(2) Å; and Cu2−N4, 1.996(2) Å. Selected bond angles: O1−Cu2−S1, 85.91(5)°; O1−Cu2−N1, 90.07(7)°; O1−Cu2−N3, 97.06(8)°; O1−Cu2−N4, 153.06(8)°; N1−Cu2−S1, 171.50(6)°; N1−Cu2−N3, 82.83(8)°; N3−Cu2−S1, 105.08(6)°; N4−Cu2−S1, 98.45(7)°; N4−Cu2−N1, 81.83(8)°; N4−Cu2−N3, 107.27(9)°; O1−Cu1−N8, 91.60(7)°; O1−Cu1−N6, 87.77(7)°; O1−Cu1−N2, 91.55(7)°; O1−Cu1−N5, 161.72(7)°; N8−Cu1−N6, 115.38(8)°; N8−Cu1−N2, 164.40(7)°; N8−Cu1−N5, 92.06(8)°; N2−Cu1−N6, 80.01(8)°; N5−Cu1−N6, 106.73(8)°; and N5−Cu1−N2, 80.40(8)°.

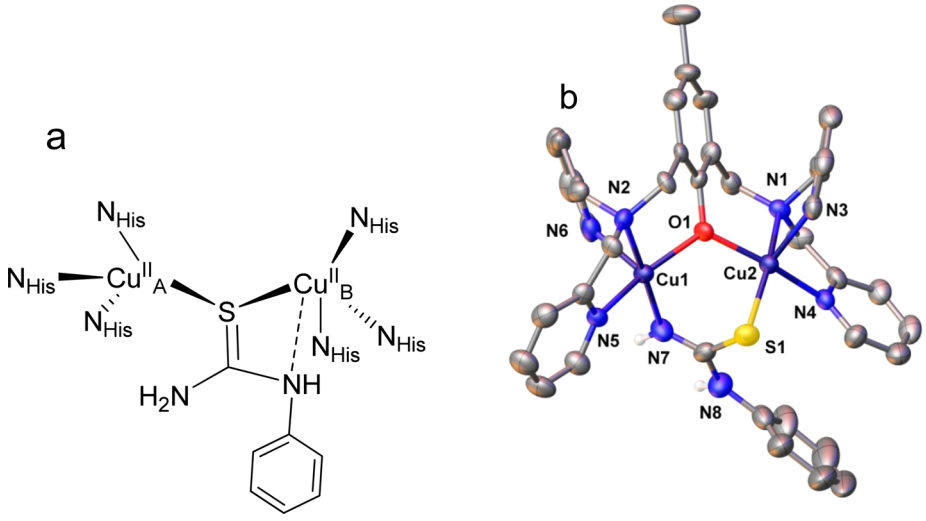

Figure 5. (a) Schematic representation (redrawn from ref 5a) of active site region of catechol oxidase from sweet potatoes (*Ipomoea batatas*) with bound PTU and selected bond lengths (CuA−S, 2.33 Å; CuB−S, 2.26 Å; CuA−*N*-thioamide, 2.58 Å; C−S, 1.61 Å; CuA···CuB, 4.22 Å). (b) Molecular structure of the cation of **1**-PTU. Hydrogen atoms (except for nitrogen from PTU), counterions and solvent molecules have been omitted for clarity. Selected bond lengths for **1**-PTU: Cu1···Cu2, 3.469 Å; Cu1−O1, 2.013(6) Å; Cu1−N6, 2.198(9) Å; Cu1−N7, 1.971(8) Å; Cu1−N2, 2.063(8) Å; Cu1−N5, 2.036(8) Å; Cu2−S1, 2.325(3) Å; Cu2−O1, 1.968(7) Å; Cu2−N1, 2.096(8) Å; Cu2−N4, 2.019(8) Å; and Cu2−N3, 2.172(8) Å. Selected bond angles for **1**-PTU: O1−Cu1−N6, 90.9(3)°; O1−Cu1−N2, 91.6(3)°; O1−Cu1−N5, 161.2(3)°; N7−Cu1−O1, 91.5(3)°; N7−Cu1−N6, 101.1(4)°; N7−Cu1−N2, 175.5(3)°; N7−Cu1−N5, 95.0(3)°; N2−Cu1−N6, 82.2(3)°; N5−Cu1−N6, 105.1(3)°; N5−Cu1−N2, 81.1(3)°; O1−Cu2−S1, 88.97(19)°; O1−Cu2−N1, 91.0(3)°; O1−Cu2−N4, 163.9(3)°; O1−Cu2−N3, 90.6(3)°; N1−Cu2−S1, 166.4(2)°; N1−Cu2−N3, 83.1(3)°; N4−Cu2−S1, 95.6(2)°; N4−Cu2−N1, 81.0(3)°; N4−Cu2−N3, 102.1(3)°; and N3−Cu2−S1, 110.4(2)°.

associated with one THF molecule were obtained together with dark green crystals of complex **1**.

Pure **1**-PTSC and **1**-PTU adducts have each been collected crystal by crystal (see the Experimental Section) from the crystallization batches. ESI-MS spectra of isolated complexes **1**-PTSC and **1**-PTU provide fragments at m/z = 934 (z = 1, $[Cu_2(BPMP)(PTSC)](ClO_4)^+$) and m/z = 906 (z = 1, $[Cu_2(BPMP)(PTU)](ClO_4)^+$) for **1**-PTSC and **1**-PTU,

dx.doi.org/10.1021/ic501829s | *Inorg. Chem.* 2014, 53, 12848−12858

Chart 2. PTSC and PTU Adducts Isolated and X-ray Characterized after Binding on Model Complex 1

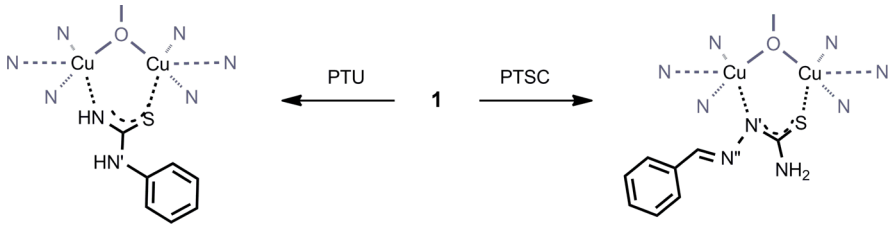

respectively (see Figures S10 and S11 in the ESI with the observed/theoretical isotopic patterns distribution). As previously observed with the initial complex $[Cu_2(\mu\text{-BPMP})(\mu\text{-OH})](ClO_4)_2$,[19] the isolated complexes **1**-PTU and **1**-PTSC are EPR silent in frozen solution (1 mM at 100 K, H_2O/DMSO (70/30, v/v, buffered at pH 7 (HEPES 100 mM)), which indicates a strong antiferromagnetic coupling ($S = 0$) ground spin state between the two copper(II) atoms for both. This observation is consistent with a doubly bridged structure and a short Cu−Cu distance, as evidenced in the solid state for **1**-PTU and **1**-PTSC (see below).

In order to gain more insight into the magnetic properties of the complexes,[33] DFT calculations were undertaken on the crystal structures of complexes **1**-PTU and **1**-PTSC. The computed values of the $2J$ exchange coupling for complexes **1**-PTU and **1**-PTSC, calculated using a broken symmetry approach,[34] are -161 cm^{-1} and -116 cm^{-1}, respectively. Magnetic orbitals for the broken symmetry state are given in Figure S12 in the ESI, showing an antiferromagnetic coupling between the two Cu atoms through the O atoms of the Cu_2O_2 core. For comparison, for complex **1**, the exchange coupling obtained from experimental magnetic studies is $2J = -156 \pm 6$ cm^{-1}.[19]

X-ray Crystallography. All the crystal-structure parameters are given in the Experimental Section. A view of the dications **1**-$PTSC^{2+}$ and **1**-PTU^{2+}, and selected bond lengths and angles, are shown in Figures 4 and 5, respectively. Both structures clearly evidence that PTU and PTSC bind the dicopper center as bidentate and bridging ligands replacing the μ-hydroxido ligand in **1**. Interaction between inhibitor PTSC or PTU with the dicopper center is in a 1:1 stoichiometry while the spectrophotometry study (done at a different concentration and in a different solvent) indicates that the predominant species is the 1:2 stoichiometry.

Complex **1**-PTSC crystallizes as $[Cu_2(\mu\text{-BPMP})(\mu\text{-PTSC-}\kappa N':\kappa S)](ClO_4)_2\cdot(C_3H_6O)_2$ (Figure 4b) with two associated acetone molecules in the presence of green crystals corresponding to complex **1**, where the bridging OH has been replaced by a bridging perchlorate (Figure 4a) and the dicopper center is in a $Cu^{II}Cu^{I}$ mixed-valent state (X-ray description and selected bond lengths and angles are given in the ESI). Crystals of $[Cu_2(\mu\text{-BPMP})(\mu\text{-PTU-}\kappa N:\kappa S)](ClO_4)_2\cdot(THF)$ (**1**-PTU) contain one associated THF molecule. In **1**-PTSC, the bridging monodeprotonated TSC increases the Cu−Cu distance from ∼2.9 Å in complex **1** to 3.378 Å. Both Cu atoms display a distorted square pyramidal geometry (Cu1: τ = 0.04, Cu2: τ = 0.3)[35] whose apical positions are occupied by the pyridine nitrogen N6 and N3, respectively. Adduct **1**-PTU possesses a similar coordination environment but slightly more distorted square pyramidal geometry (Cu1: τ = 0.24, Cu2: τ = 0.4).[35] The square plane in **1**-PTSC is defined by N2, N5, N8, and O1 atoms for Cu1 and O1, N1, N4, S1 atoms for Cu2 and in **1**-PTU by N2, N5, N7 and O1 atoms for Cu1 and O1, N1, N4, S1 atoms for Cu2. The Cu1−O1−Cu2 bond angles are in the same range (118.16° for **1**-PTSC and 121.32° for **1**-PTU).

In **1**-PTSC, by comparison with **1**-PTU, the Cu2−S1 (2.370 Å) and the Cu1−N8 (2.029 Å) distances are longer than the one observed in **1**-PTU (see Figure 5b) (Cu2−S1 (2.325 Å) and the Cu1−N8 (1.971 Å). Besides, the C−S1 distances are significantly longer (1.740 Å for both), indicating the increased single-bond character expected in deprotonated forms. In the reported *Ib*CO-PTU structure,[5a] the C−S1 distance of 1.61 Å is in accordance with a thione neutral form.[36] Consequently, the PTU binding mode observed is different from the one reported on structural data from *Ib*CO and bound phenylthiourea (Figure 5a).[5a] For both, PTU replaces the bridging hydroxido increasing the Cu−Cu separation from ∼2.9 Å to 3.469 Å on **1**-PTU and to 4.22 Å on *Ib*CO-PTU.

In **1**-PTU, the observed binding mode results in deprotonation of the amine group interacting with one Cu atom and the interaction of the S atom with the other Cu atom while on *Ib*CO-PTU; the preferential incorporation of the S atom in the bridge in a neutral form is associated with a weak interaction of the thioamide N atom with one Cu atom (CuB−N distance = 2.58 Å; see Figure 5a). The observed bridging mode of PTSC is related to the one observed in **1**-PTU but differs from other structurally characterized TSCs[13f] bound on binuclear copper complexes. In summary, the molecular structure of **1**-PTSC and **1**-PTU adducts determined by single-crystal XRD analysis are shown for both an unusual bridging binding mode on the dicopper center (see Chart 2). From both previous and present work, binding mode studies of different Ty inhibitors with complex **1** afford a multiplicity of isolated and X-ray characterized adducts (recall Chart 1), demonstrating the potential of complex **1** to stabilize Cu_2-inhibitor adducts.

Copper coordination is modulated by geometric consideration of inhibitors and not by the nature of the donor setting, since both HOPNO and KA (O/O donors) afforded different binding modes. Despite a slightly different binding motif for PTSC and PTU, the binding mode is similar. All these inhibitors bind in a bidendate fashion to one or both copper in their adduct with complex **1**, both requiring a deprotonation step of the linker, emphasizing the importance to tune pK_a on potential new tyrosinase inhibitors targeting the dicopper center. These results clearly illustrate how the geometry and composition of the dinuclear center in **1** bringing the Cu ions closer, affects the binding and support the coordination versatility of PTU and PTSC.

Computational Studies. Furthermore, the X-ray structures of **1**-$PTSC^{2+}$ and **1**-PTU^{2+} help us to explore the interactions of PTSC and PTU in the enzymatic active site using the recently resolved X-ray structure of *Agaricus bisporus* mushroom tyrosinase (PDB code: 2Y9X).[2a] Docking of the ligands in the enzyme was performed manually. For that, an alignment

dx.doi.org/10.1021/ic501829s | *Inorg. Chem.* 2014, 53, 12848−12858

was performed between the Nε nitrogen from histidine and the Cu atoms of the enzyme, the pyridine nitrogen, and the Cu atoms of **1**-PTSC^{2+} and **1**-PTU^{2+}. The systems were then solvated and molecular mechanic simulations were performed (see computation details in the Experimental Section). Stable structures were found for the two systems, close for the two molecules. For both, distances between the Cu atoms and the inhibitors are significantly longer than the distances found with the model complex, as expected for a description by molecular mechanics, which does not depict covalent interactions between molecules and metallic ions. For PTSC, the Cu−S average distances are 2.55 and 2.77 Å (2.47 and 2.77 Å, respectively, for PTU). The Cu−N8 average distance for PTSC (Cu−N7 for PTU) is equal to 4.44 Å (4.33 Å for PTU). In Figure 6, the structure obtained for PTSC is given (see Figure S13 in the ESI for PTU). Nonbound interactions between the aromatic ring of PTSC and three residues (Val247, Asn259, and His243) close to the active site are highlighted.

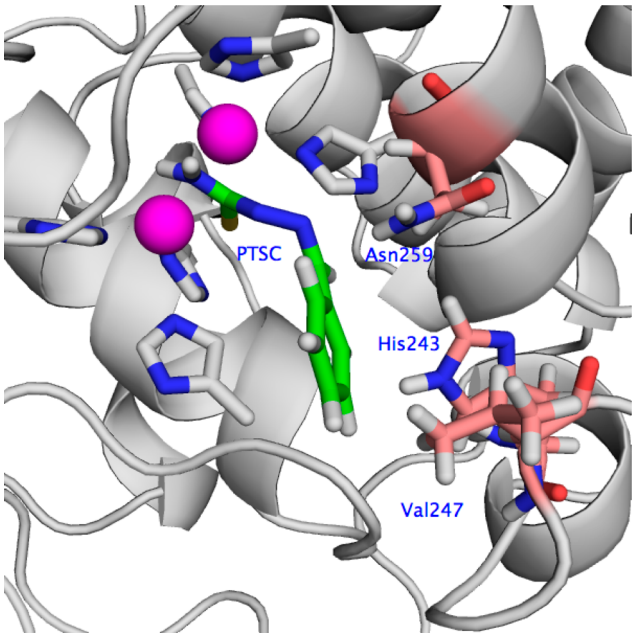

Figure 6. Binding mode of PTSC after 2 ns of MM dynamics on *Agaricus bisporus* mushroom tyrosinase (PDB code: 2Y9X).[2a] Carbon atoms of PTSC are illustrated in green, copper atoms in magenta, carbon atoms of the three residues at 3 Å of the aromatic cycle of PTSC in pale pink, nitrogen atoms in blue, sulfur atoms in yellow, and oxygen atoms in red.

The estimation of the binding free energies was computed with the inclusion of solvation effects via Poisson−Boltzmann/surface area calculations, namely, MM-PBSA.[37] A similar evaluation has already been performed on docked positions of thujaplicins on a homology model of TyM.[38] The calculated binding free energies (ΔG_{calc} = −14.0 ± 3.5 kcal/mol for PTCS versus −0.1 ± 2.3 kcal/mol for PTU) matched the experimental order of inhibition efficiency well (PTSC > PTU).

CONCLUSIONS

We have reported a description of two inhibitors for mushroom Tyrosinase (Ty), phenylmethylene thiosemicarbazone (PTSC), and phenylthiourea (PTU). At an enzymatic level, both compounds exhibit mainly competitive inhibition, with a small contribution of uncompetitive behavior (large K_{IU}/K_{IC}), which evidence that these compounds interact in the active site of the enzyme. With a K_{IC} value of 0.93 μM, PTSC is one of the best mushroom Ty inhibitors described in the literature. In addition, computational studies confirm that PTSC and PTU interact with the metal center of the active site. The estimation of the binding free energies inhibitors/Ty confirms the high inhibitor efficiency of PTSC. Taking advantage of above information, we can initiate a structure−activity relationship exploration of PTSC derivatives toward mushroom Ty inhibition to design inhibitors that are much more efficient. Additionally, the nature of the aromatic nucleus bearing the coordinating moieties is also of importance as pointed from our preliminary results (see Table S1 in the Supporting Information) after the introduction of a fluorine atom in *met* or *para* position on the phenyl ring on PTSC or replacement of the aromatic nucleus by a heterocycle. This is in accordance with previously reported results[12a,i,j] as a strategy to modulate the inhibition properties.

At the coordination chemistry level, we have used a dinuclear Cu^{II} complex to analyze possible interaction modes with PTU and PTSC. As evidenced by the X-ray crystal structures, PTU and PTSC unambiguously bind as bridged, bidentate and monodeprotonated ligands on the dinuclear center from complex **1**, demonstrating, at the same time, a unique and distinct binding mode compared to the one observed in an X-ray structure of PTU bound on the enzyme catechol oxidase. So, a direct extrapolation of the observed binding mode on model complexes to interaction with the tyrosinase active site is hazardous as in the enzyme other interactions including hydrogen bonding, hydrophobic or van der Waals interactions can influence inhibitor coordination to the active site as pointed us by a simulation, showing important second-sphere interactions PTSC with, in particular, the three residues Val247, Asn259, and His243 in the enzyme. Despite the limitations of model complexes in binding prediction, we have shown their utility as a starting point in modeling studies. Furthermore, model complex studies pointed out the adaptable binding mode of PTU and PTSC on a dicopper center and important parameters controlling the binding geometry around the dicopper center or protonation state. These insights into the interplay between the inhibitor binding and the copper coordination emphasize its importance and gives guidance regarding inhibitor design for the development of new Ty inhibitors. It is of particular interest, considering the importance of selective Ty inhibition in medicinal and dermato-cosmetic fields. Studies are currently in progress in our laboratories to prepare and evaluate new multimodal compounds for selective and efficient Ty inhibition.

ASSOCIATED CONTENT

Supporting Information

Picture of the crystallization batch from where **1**-PTSC·$2C_3H_6O$ was recovered; bond lengths (Å) and angles (deg) for **1**-ClO_4·C_4H_8O·H_2O and X-ray description; titration of complex **1** by PTU and PTSC; enzymatic data for the mushroom Ty inhibition by PTSC and PTU (Figures S4−S8 and Table S1); ESI-MS and HR-ESI-MS data; magnetic orbitals for the broken symmetry state of complexes **1**-PTSC and **1**-PTU; binding mode of PTU after MM dynamics. CIF files for **1**-PTSC·$2C_3H_6O$, **1**-ClO_4·C_4H_8O·H_2O, and **1**-PTU·C_4H_8O. This material is available free of charge via the Internet at http://pubs.acs.org.

AUTHOR INFORMATION

Corresponding Authors

*Tel.: +33-491288823. E-mail: marius.reglier@univ-amu.fr.
*Tel.: +33-476514838. E-mail: catherine.belle@ujf-grenoble.fr.

Present Addresses

[∇]Centre de Biophysique Moléculaire, UPR 4301, Orléans, France.
[∥]Shanghai Institute of Materia Medica, Chinese Academy of Sciences, Shanghai, PRC.

Notes

The authors declare no competing financial interest.

ACKNOWLEDGMENTS

Financial support and E.B. postdoctoral fellowship by the Labex ARCANE (ANR-11-LABX-0003-01) are gratefully acknowledged. The authors acknowledge support from ICMG FR 2607, ANR (Agence Nationale pour la Recherche, Program Blanc 2Cu-TargMelanin (No. ANR-09-BLAN-0028-01/02/03) and the European COST Program in the framework of which this work was carried out (COST action CM1003 WG 2).

REFERENCES

(1) (a) Solomon, E. I.; Sudaram, U. M.; Mackonkin, T. E. *Chem. Rev.* **1996**, *96*, 2563−2605. (b) Gerdemann, C.; Eicken, C.; Krebs, B. *Acc. Chem. Res.* **2002**, *35*, 7019−7022. (c) Belle, C. In *Encyclopedia of Metalloproteins*; Kretsinger, R. H., Uversky, V. N., Permyakov, E. A., Eds.; Springer−Verlag: Berlin, Heidelberg, 2013; pp 574−579. (d) Tepper, A. W. J. W.; Lonardi, E.; Bubacco, L.; Canters, G. W. In *Handbook of Metalloproteins*, Vol. 5; Messerschmidt, A., Ed.; Wiley: Chichester, U.K., **2011**; pp 571−587. (e) Rolff, M.; Schottenheim, J.; Decker, H.; Tuczek, F. *Chem. Soc. Rev.* **2011**, *40*, 4077−4098. (f) Solomon, E. I.; Heppner, D. E.; Johnston, E. M.; Ginsbach, J. W.; Cirera, J.; Quyyum, M.; Kieber-Emmons, M. T.; Kjaergaard, C. H.; Hadt, R. G.; Tian, L. *Chem. Rev.* **2014**, *114*, 3659−3853. (g) Ramsden, C. A.; Riley, P. A. *Biorg. Med. Chem.* **2014**, *22*, 2388−2395.

(2) (a) Ismaya, W. T.; Rozeboom, H. J.; Weijn, A.; Mes, J. J.; Fusetti, F.; Wichers, H. J.; Dijkstra, B. *Biochemistry* **2011**, *50*, 5477−5486. (b) Hakulinen, N.; Gasparetti, C.; Kaljunen, H.; Kruus, K.; Rouvinen, J. *J. Biol. Inorg. Chem.* **2013**, *18*, 917−929. (c) Haudecoeur, R.; Gouron, A.; Dubois, A.; Jamet, H.; Lightbody, M.; Hardré, R.; Milet, A.; Bergantino, E.; Bubacco, L.; Belle, C.; Réglier, M.; Boumendjel, A. *ChemBioChem* **2014**, *15*, 1325−1333. (d) Favre, E.; Daina, A.; Carrupt, P.-A.; Nurisso, A. *Chem. Biol. Drug Des.* **2014**, *84*, 206−215. (e) Selinheimo, E.; NiEidhin, D.; Steffensen, C.; Nielsen, J.; Lomascolo, A.; Halaoui, S.; Record, E.; O'Beirne, D.; Buchert, J.; Kruus, K. *J. Biotechnol.* **2007**, *130*, 471−480. (f) Matoba, Y.; Kumagai, T.; Yamamoto, A.; Yoshitsu, H.; Sugiyama, M. *J. Biol. Chem.* **2006**, *281*, 8981−8990.

(3) Fujieda, S.; Yabuta, S.; Ikeda, T.; Oyama, T.; Muraki, N.; Kurisu, G.; Itoh, S. *J. Biol. Chem.* **2013**, *288*, 22128−22140.

(4) Sendovski, M.; Kanteev, M.; Shuster Ben-Yosef, V.; Adir, N.; Fishman, A. *J. Mol. Biol.* **2011**, *405*, 227−237.

(5) (a) Klabunde, T.; Eicken, C.; Sacchettini, J. C.; Krebs, B. *Nat. Struct. Biol.* **1998**, *5*, 1084−1090. (b) Virador, V. M.; Grajeda, J. P. R.; Blanco-Labra, A.; Mendiola-Olaya, E.; Smith, G. M.; Moreno, A.; Whitaker, J. R. *J. Agric. Food Chem.* **2010**, *58*, 1189−1201.

(6) Ito, S.; Wakamatsu, K. *Photochem. Photobiol.* **2008**, *84*, 582−592.

(7) Loizzo, M. R.; Tundis, R.; Menichini, F. *Compr. Rev. Food. Sci. Food. Saf.* **2012**, *11*, 378−398.

(8) Solano, F.; Briganti, S.; Picardo, M.; Ghanem, G. *Pigment Cell Res.* **2006**, *19*, 550−571.

(9) (a) Chang, T. S. *Int. J. Mol. Sci.* **2009**, *10*, 2440−2475. (b) Mendes, E.; Perry, M. d. J.; Franscisco, A. P. *Expert Opin. Drug Discovery* **2014**, *9*, 533−554.

(10) (a) Criton, M.; Le Mellay-Hamon, V. *Bioorg. Med. Chem. Lett.* **2008**, *18*, 3607−3610. (b) DuBois, K. P.; Erway, W. F. *J. Biol. Chem.* **1946**, *165*, 711−721.

(11) Eicken, C.; Zippel, F.; Büldt-Karentzopoulos, K.; Krebs, B. *FEBS Lett.* **1998**, *436*, 293−299.

(12) (a) Li, Z.-C.; Chen, L.-H.; Yu, X.-J.; Hu, Y.-H.; Song, K.-K.; Zhou, X.-W.; Chen, Q.-X. *J. Agric. Food Chem.* **2010**, *58*, 12537−12540. (b) Chen, L.-H.; Hu, Y.-H.; Song, W.; Song, K.-K.; Liu, X.; Jia, Y.-L.; Zhuang, J.-X.; Chen, Q.-X. *J. Agric. Food Chem.* **2012**, *60*, 1542−1547. (c) Pan, Z.-Z.; Zhu, Y.-J.; Yu, X.-J.; Lin, Q.-F.; Xiao, R.-F.; Tang, J.-Y.; Chen, Q.-X.; Liu, B. *J. Agric. Food Chem.* **2012**, *60*, 10784−10788. (d) Liu, J.; Yi, W.; Wan, Y.; Ma, L.; Song, H. *Bioorg. Med. Chem.* **2008**, *16*, 1096−1102. (e) Liu, J.; Cao, R.; Yi, W.; Ma, C.; Wan, Y.; Zhou, B.; Ma, L.; Song, H. *Eur. J. Med. Chem.* **2009**, *44*, 1773−1778. (f) Yi, W.; Cao, R.; Wen, H.; Yan, Q.; Zhou, B.; Ma, L.; Song, H. *Bioorg. Med. Chem. Lett.* **2009**, *19*, 6157−6160. (g) Xue, C.-B.; Zhang, L.; Luo, W.-C.; Xie, X.-Y.; Jiang, L.; Xiao, T. *Bioorg. Med. Chem.* **2007**, *15*, 2006−2015. (h) Yi, W.; Cao, R.-H.; Chen, Z.-Y.; Yu, L.; Ma, L.; Song, H.-C. *Chem. Pharm. Bull.* **2009**, *57*, 1273−1277. (i) Yi, W.; Cao, R.; Chen, Z.; Yu, L.; Wen, H.; Yan, Q.; Ma, L.; Song, H. *Chem. Pharm. Bull.* **2010**, *58*, 752−754. (j) Yi, W.; Dubois, C.; Yahiaoui, S.; Haudecoeur, R.; Belle, C.; Song, H.; Hardré, R.; Réglier, M.; Boumendjel, A. *Eur. J. Med. Chem.* **2011**, *46*, 4330−4335.

(13) (a) West, D. X.; Liberta, A. E.; Padhye, S. B.; Chikate, R. C.; Sonawane, P. B.; Kumbhar, A. S.; Yerande, R. G. *Coord. Chem. Rev.* **1993**, *123*, 49−71. (b) Beraldo, H.; Gambino, D. *Mini-Rev. Med. Chem.* **2004**, *4*, 31−39. (c) Tisato, F.; Marzano, C.; Porchia, M.; Pellei, M.; Santini, C. *Med. Res. Rev.* **2010**, *30*, 708−749. (d) Casas, J. S.; García-Tasende, M. S.; Sordo, J. *Coord. Chem. Rev.* **2000**, *209*, 197−261. (e) Paterson, B. M.; Donnelly, P. *Chem. Soc. Rev.* **2011**, *40*, 3005−3018. (f) Lobana, T. S.; Sharma, R.; Bawa, G.; Khanna, S. *Coord. Chem. Rev.* **2009**, *253*, 977−1055.

(14) (a) Lee, K. C.; Thanigaimalai, P.; Sharma, R.; Kim, M. S.; Roh, E.; Hwang, B. Y.; Kim, Y.; Jung, S. H. *Bioorg. Med. Chem. Lett.* **2010**, *20*, 6794−6796. (b) Thanigaimalai, P.; Hoang, T. A. L.; Lee, K. C.; Bang, S. C.; Sharma, V. K.; Yun, C. Y.; Roh, E.; Hwang, B. Y.; Kim, S. H. *Biorg. Med. Chem. Lett.* **2010**, *20*, 2991−2993.

(15) (a) Wöckel, S.; Galezowska, J.; Dechert, S.; Meyer, F. *Inorg. Chem.* **2012**, *51*, 2486−2493. (b) Rouffet, M.; Cohen, S. M. *Dalton Trans.* **2011**, *40*, 3445−3453. (c) Bochot, C.; Favre, E.; Dubois, C.; Baptiste, B.; Bubacco, L.; Carrupt, P.-A.; Gellon, G.; Hardré, R.; Luneau, D.; Moreau, Y.; Nurisso, A.; Réglier, M.; Serratrice, G.; Belle, C.; Jamet, H. *Chem.—Eur. J.* **2013**, *19*, 3655−3664.

(16) (a) Koval, I. A.; Gamez, P.; Belle, C.; Selmeczi, K.; Reedijk, J. *Chem. Soc. Rev.* **2006**, *35*, 814−840. (b) Selmeczi, K.; M, R.; Giorgi, M.; Speier, G. *Coord. Chem. Rev.* **2003**, *245*, 191−201.

(17) Peyroux, E.; Ghattas, W.; Hardré, R.; Giorgi, M.; Faure, B.; Simaan, A. J.; Belle, C.; Réglier, M. *Inorg. Chem.* **2009**, *48*, 10874−10876.

(18) Bochot, C.; Gouron, A.; Bubacco, L.; Milet, A.; Philouze, C.; Réglier, M.; Serratrice, G.; Jamet, H.; Belle, C. *Chem. Commun.* **2014**, *50*, 308−310.

(19) Torelli, S.; Belle, C.; Gautier Luneau, I.; Pierre, J. L.; Saint Aman, E.; Latour, J. M.; Le Pape, L.; Luneau, D. *Inorg. Chem.* **2000**, *39*, 3526−3536.

(20) (a) Lobana, T. S.; Rekha; Butcher, R. J.; Castineiras, A.; Bermejo, E.; Bharatam, P. V. *Inorg. Chem.* **2006**, *45*, 1535−1542. (b) Maillard, L. T.; Bertout, S.; Quinonéro, O.; Akalin, G.; Turan-Zitouni, G.; Fulcrand, P.; Demirci, F.; Martinez, J.; Masurier, N. *Bioorg. Med. Chem. Lett.* **2013**, *23*, 1803−1807.

(21) (a) Gampp, H.; Maeder, M.; Meyer, C. J.; Zuberbühler, A. D. *Talanta* **1985**, *32*, 95−101. (b) Gampp, H.; Maeder, M.; Meyer, C. J.; Zuberbühler, A. D. *Talanta* **1985**, *32*, 257−264. (c) Gampp, H.; Maeder, M.; Meyer, C. J.; Zuberbühler, A. D. *Talanta* **1986**, *33*, 943−951.

(22) Sheldrick, G. M. *Acta Crystallogr., Sect. A: Found. Crystallogr.* **2008**, *A64*, 112−122.

(23) Dolomanov, O. V.; Bourhis, L. J.; Gildea, R. J.; Howard, J. A. K.; Puschmann, H. *J. Appl. Crystallogr.* **2009**, *42*, 339−341.

(24) *TWINABS, Scaling and corrections for twinned crystals*; Version 1.05, Bruker Nonius.
(25) Yamazaki, S.; Itoh, S. *J. Am. Chem. Soc.* **2003**, *125*, 13034−13035.
(26) Frisch, M. J.; Trucks, G. W.; Schlegel, H. B.; Scuseria, G. E.; Robb, M. A.; Cheeseman, J. R.; Scalmani, G.; Barone, V.; Mennucci, B.; Petersson, G. A.; Nakatsuji, H.; Carito, M.; Li, X.; Hratchian, H. P.; Izmaylov, A. F.; Bloino, J.; Zheng, G.; Sonnenberg, J. L.; Hada, M.; Ehara, M.; Toyota, K.; Fukuda, R.; Hasegawa, J.; Ishida, M.; Nakajima, T.; Honda, Y.; Kitao, O.; Nakai, H.; Vreven, T.; Montgomery, J. A.; Peralta, J. E.; Ogliaro, F.; Bearpark, M.; Heyd, J. J.; Brothers, E.; Kudin, K. N.; Staroverov, V. N.; Kobayashi, R.; Normand, J.; Raghavachari, K.; Rendell, A.; Burant, J. C.; Iyengar, S. S.; Tomasi, J.; Cossi, M.; Rega, N.; Millam, J. M.; Klene, M.; Knox, E.; Cross, J. B.; Bakken, V.; Adamo, C.; Jaramillo, J.; Gomperts, R.; Stratmann, R. E.; Yazyev, O.; Austin, A. J.; Cammi, R.; Pomelli, C.; Ochterski, J.; Martin, R. L.; Morokuma, K.; Zakrzewski, V. G.; Voth, G. A.; Salvador, P.; Dannenberg, J. J.; Dapprich, S.; Daniels, A. D.; Farkas, O.; Foresman, J. B.; Ortiz, J. V.; Cioslowski, J.; Fox, D. J. *Gaussian 09, Revision D01*; Gaussian, Inc.: Wallingford, CT, 2009.
(27) Soda, T.; Kitagawa, Y.; Onishi, T.; Takano, Y.; Shigeta, Y.; Nagao, H.; Yoshika, Y.; Yamaguchi, K. *Chem. Phys. Lett.* **2000**, *319*, 223−230.
(28) *SYBYL 8.0*; Tripos Associates, Inc.: St. Louis, MO, 2007.
(29) Case, D. A.; Darden, T. A.; Cheatham, T. E.; Simmerling, C. L.; Wang, J.; Duke, R. E.; Luo, R.; Walker, R. C.; Zhang, W.; Merz, K. M.; Roberts, B. S.; Roitberg, A.; Seabra, G.; Swails, J.; Götz, A. W.; Kolossvary, I.; Wong, K. F.; Paesani, F.; Vanicek, J.; Wolf, R. M.; Liu, J.; Wu, X.; Brotzell, S. R.; Steinbrecher, T.; Gohlke, H.; Cai, Q.; Ye, X.; Wang, J.; Hsieh, M.-J.; Cui, G.; Roe, D. R.; Mathews, D. H.; Seetin, M. G.; Salomon-Ferrer, R.; Sagui, C.; Babin, V.; Luchko, T.; Gusarov, S.; Kovalenko, A.; Kollman, P. A. *Amber 12*; University of California: San Francisco, CA, 2012.
(30) Cornish-Bowden, A. *Fundamentals of Enzyme Kinetics*; Portland Press: London, 1995.
(31) Dubois, C.; Haudecoeur, R.; Orio, M.; Belle, C.; Bochot, C.; Boumendjel, A.; Hardré, R.; Réglier, M. *ChemBioChem* **2012**, *13*, 559−565.
(32) (a) Ghani, U.; Ullah, N. *Biorg. Med. Chem.* **2010**, *18*, 4042−4048. (b) Chen, J. S.; Wei, C.; Marshall, M. R. *J. Agric. Food Chem.* **1991**, *39*, 1897−1901.
(33) Because of the easy **1**-PTU and **1**-PTSC dissociation in solution and the excess of inhibitors necessary, all of our attempts to recover a sufficient amount of pure adduct in solid state to perform additional experimental studies as magnetic studies have failed.
(34) (a) Noodleman, L. *J. Chem. Phys.* **1981**, *74*, 5737−5743. (b) Noodleman, L.; Case, D. A. *Adv. Inorg. Chem.* **1992**, *38*, 423−470. (c) Noodleman, L.; Davidson, E. R. *Chem. Phys.* **1986**, *109*, 131−143.
(35) Addison, A. W.; Rao, T. N.; Reedijk, J.; van Rijn, J.; Verschoor, G. *J. Chem. Soc., Dalton Trans.* **1984**, 1349−1356.
(36) (a) Duan, C.-H.; Wu, B.-M.; Mak, T. C. W. *J. Chem. Soc., Dalton Trans.* **1996**, 3485−3490. (b) Villa, A. C.; Manfredotti, A. G.; Guastini, C. *Cryst. Struct. Commun.* **1972**, *1*, 207−208. (c) Bingham, A. G.; Bögge, H.; Müller, A.; Ainscough, E. W.; Brodie, A. M. *J. Chem. Soc., Dalton Trans.* **1987**, 493−499.
(37) Kollman, P. A.; Massova, I.; Reyes, C.; Kuhn, B.; Huo, S.; Chong, L.; Lee, M.; Lee, T.; Duan, Y.; Wang, W.; Donini, O.; Cieplak, P.; Srinivasan, J.; Case, D. A.; Cheatham, T. E. *Acc. Chem. Res.* **2000**, *33*, 889−897.
(38) Takahashi, S.; Kamiya, T.; Saeki, K.; Nezu, T.; Takeuchi, S.-I.; Takasawa, R.; Sunaga, S.; Yoshimori, A.; Ebikura, S.; Abe, T.; Tanuma, S. *Bioorg. Med. Chem.* **2010**, *18*, 8112−8118.